Best-fit results from application of a thermo-rheological model for channelized lava flow to high spatial resolution morphological data

Andrew Harris[1], Massimiliano Favalli[2], Francesco Mazzarini[2], Maria Teresa Pareschi[2]

[1]*Hawaii Institute of Geophysics and Planetology, School of Oceanography and Earth Science Technology, University of Hawaii, 1680 East-West Road, Honolulu, USA*

[2]*Istituto Nazionale di Geofisica e Vulcanologia, Via della Faggiola 32, Pisa, ITALY*

Abstract.

The FLOWGO thermo-rheological model links heat loss, core cooling, crystallization, rheology and flow dynamics for lava flowing in a channel. We fit this model to laser altimeter (LIDAR) derived channel width data, as well as effusion rate and flow velocity measurements, to produce a best-fit prediction of thermal and rheological conditions for lava flowing in a ~1.6 km long channel active on Mt. Etna (Italy) on 16th September 2004. Using, as a starting condition for the model, the mean channel width over the first 100 m (6 m) and a depth of 1 m we obtain an initial velocity and instantaneous effusion rate of 0.3-0.6 m/s and ~3 m^3/s, respectively. This compares with field- and LIDAR-derived values of 0.4 m/s and 1-4 m^3/s. The best-fit between model-output and LIDIR-measured channel widths comes from a hybrid run in which the proximal section of the channel is characterised by poorly insulated flow and the medial-distal section by well-insulated flow. This best-fit model implies that flow

conditions evolve down-channel, where hot crusts on a free flowing channel maximise heat losses across the proximal section, whereas thick, stable, mature crusts of 'a'a clinker reduce heat losses across the medial-distal section. This results in core cooling per unit distance that decreases from ~0.02-0.015 °C m^{-1} across the proximal section, to ~0.005 °C m^{-1} across the medial-distal section. This produces an increase in core viscosity from ~3800 Pa s at the vent to ~8000 Pa s across the distal section.

INTRODUCTION

By controlling core cooling and crystallization, lava flow heat loss provides a powerful control on flow rheology hence flow dynamics, morphology and dimensions [e.g. *Pieri and Baloga*, 1986; *Kilburn and Lopes*, 1988; *Dragoni*, 1989; *Fink and Griffiths*, 1992; *Dragoni and Tallarico*, 1994; *Pinkerton and Wilson*, 1994; *Crisp and Baloga*, 1994; *Cashman et al.*, 1999; *Gregg and Fink*, 2000; *Quareni et al.*, 2004]. FLOWGO is a thermo-rheological model that aims to link heat loss, core cooling and crystallization, rheology and, hence, flow dynamics for lava flowing in a channel [*Harris and Rowland*, 2001]. The model takes a control volume of lava and moves this down-channel while applying a heat loss model that considers radiation and convection from the flow surface, and conduction through the base. This is used to calculate the core cooling and crystallization rate, which is in-turn used to apply the temperature and crystal dependent viscosity and yield strength relationships given by *Dragoni* [1989] and *Pinkerton and Stevenson* [1992]. This, finally, is used to solve Jeffreys Equation [*Jeffreys*, 1925], modified for a Bingham fluid flowing in a semi-circular and/or wide channel following *Moore* [1987], to assess flow velocity at each step. Lava with new

thermal and rheological properties are then passed onto the next step and the model is run iteratively until cooling forces the control volume to a point where it is rheologically incapable of flow.

In running the model, the main controls are the starting thermo-rheological conditions (lava eruption temperature, crystallinity, viscosity and yield strength), the channel dimensions and surface thermal structure. Surface thermal structure (i.e. the extent and temperature of the surface crust) dictates the amount of insulation received by the flow interior controlling core heat loss and hence the rate of core cooling [e.g. *Keszthelyi and Self*, 1998]. As the model progresses, cooling causes viscosity and yield strength to increase, and hence velocities to decline. In order to conserve volume, the flow width and/or thickness must also increase. Thus, one way to constrain the model input parameters and to assess the validity of the output is through the use of independent data that record down-flow variation in channel dimension, as well as instantaneous effusion rate and velocity. Of these parameters, channel dimensions can now be easily acquired for an entire channel-length using, for example, LIDAR (airborne laser altimeter) data [e.g. *Mazzarini et al.*, 2005]. Instantaneous effusion rates and velocity data are largely derived from point-based measurements, applying to a specific point in time and space, but they can be used if the time and location of the measurements are known. Here we use such data from a lava channel active on Mount Etna (Sicily, Italy) during 16th September 2004 to assess the most plausible thermal and rheological flow conditions obtained from fitting the model output to the LIDAR- and field-derived morphological data.

THE 16th SEPTEMBER CHANNEL: LIDAR AND FIELD DATA

At 11:30 a.m. local time on 7th September 2004 effusive activity began near the summit of Mt. Etna to feed flows that extended towards the east (Figure 1). By 16th September, a well-defined channel had become established feeding flow extending ~1.6 km from the vent. On this date a LIDAR survey was completed using an aircraft fitted with the Optech ALTM 3033 laser altimeter [*Mazzarini et al.*, 2005; *Mazzarini et al.*, in press]. The survey covered the eastern sector of Mt. Etna and including the active flow field. This allowed construction of a Digital Elevation Model (DEM) of the area with horizontal and vertical accuracies of ±1.5 m and ±0.4 m, respectively (Figure 1). These data were reported in *Mazzarini et al.* [2005] and allowed channel profiles to be acquired every 10 m down-flow. These data defined a channel width and depth of 16 and 2 m, respectively. In addition, field measurements revealed maximum flow velocities of 0.7 m/s and instantaneous effusion rates of 2-4 m^3/s at a measurement point ~5 m from the vent [*www.ct.ingv.it/Etna2004/Default.htm*]. These compare with a time-averaged discharge rate of 2.2±0.8 m^3/s obtained from the LIDAR derived flow volume of $1.1 \times 10^6 \pm 0.4$ m^3 and an emplacement duration of ~6 days [*Mazzarini et al.*, 2005]. We next apply FLOWGO to obtain a best-fit simulation for these data for a channel within which flow was active.

MODEL-FITTING

To set up the model, there are three sets of conditions to consider: the starting thermo-rheological conditions, the channel dimensions and the surface thermal structure. We set the thermo-rheological conditions using typical values for Etnean lava

taken from the literature (Table 1). Next we fix the starting channel width at 6 m; this being the average width obtained from the LIDAR data over the first 100 m of the channel. Using a depth of 1 m, and underlying slope taken from the LIDAR-derived DEM (29 °), gives an initial velocity of 0.3-0.6 m/s. We note that, by applying *Jeffreys* [1925], this will be an average velocity for the lava flowing in the channel, and compares with the field measured maximum of 0.7 m/s; which converts to an average [following *Calvari et al.*, 2003] of 0.4 m/s. The model also gives an effusion rate of 3 m^3/s, which again compares well with the field and LIDAR-derived range of 1-4 m^3/s. It now remains to determine the surface thermal structure to define the heat loss, where all other parameters now remain fixed in all of the following model versions.

In our first set of model runs (M1) we used a high temperature model in which the surface was described by a two-component mixture model comprising cooler crust at temperature T_{crust} broken by high temperature cracks at temperature T_{crack} [*Crisp and Baloga*, 1990]. Now the effective radiation temperature of the surface (T_e) can be written $T_e = [f_{crust} T_{crust}^4 + (1- f_{crust}) T_{crack}^4]^{1/4}$, in which f_{crust} is the fractional surface area covered by crust [*Crisp and Baloga*, 1990]. We set the crust to cool as a function of time (t), where crust age is obtained from the model-derived velocity and distance from the vent. The expected crust temperature at any point in time can now be calculated following the empirically-derived surface cooling rate given by *Hon et al.* [1995], so that crust temperature (T_{crust}) = -140 x log(t)+303. Following *Harris and Rowland* [2001] we calculate fractional coverage of crust (f_{crust}) as a function of velocity (V) using f_{crust} = 0.9 exp(-0.16 x V), for a lightly crusted case (Model M1.1), or f_{crust} = 1 exp(-0.00756 x V) for a more heavily crusted case (Model M1.2) In each of these

models we set a temperature for the high temperature component (T_{crack}) that is 140 °C lower than the core temperature [*Harris and Rowland*, 2001]. Finally we run a model with no cracks (Model M1.3), i.e. f_{crust} = 1. In all three cases, the modelled channel width provides a good fit with the LIDAR-derived widths over the first 200 m of the channel length. Thereafter extreme heat losses from Model M1.1 causes the core to cool to such an extent that flow is not rheologically feasible beyond ~300 m (Figure 2a). Reduced heat losses in Models M1.2 and M1.3 provide good fits out to 460 m and 920 m, respectively, but both models stall shortly thereafter (Figure 2a). Thus flow with such a surface thermal structure cannot maintain a sufficiently fluid rheology to sustain movement along the entire channel length. In these cases, heat losses are such that core cooling forces the flow rheology to a point where flow is not feasible along the entire channel length.

Thus, in our second set of model runs (M2), we consider a cooler crust to provide improved insulation. In these models we assume a mature and stable crust at constant temperatures of ~350 °C (Model M2.1), ~250 °C (Model M2.2) and ~150 °C (Model M2.3). In all of the M2 models we simulate 100 % crust coverage (i.e. no high temperature cracks so that f_{crust} = 1). All of these models give channel widths that under-estimate the true channel width over the first 500 m (Figure 2b). However, although all of these models suppress cooling so that the flow is capable of extending further than in all of the Model 1 cases, only Model M2.3 allows lava to extend the entire channel length; providing a good fit with measured channel widths after ~700 m (Figure 2b).

However, we do not feel that such low temperature (150-350°C) and extensive crusts are appropriate for the proximal channel section. This follows the measurements of *Harris et al.* [2005] who obtained temperatures of 660-880 °C for newly formed crust on lava moving at 0.1-0.2 m/s within a proximal channel section on Etna during May 2001. Calculated crust coverage for the 3-m-wide channel was ~0.97 [*Harris et al.*, 2005]. Lower crust temperatures and 100 % coverage may, however, be appropriate for heavily crusted, medial-to-distal 'a'a flow that characterizes Etna's channel-fed flows [*Chester et al.*, 1985; *Kilburn*, 1990; *Kilburn and Guest*, 1993].

In our third set of model runs we thus applied a hybrid model (Model M3) with high and low temperature crust models operating for the proximal and medial-distal sections, respectively. Following the best-fitting hot and cold models, we thus used Models M1.2 and M2.3 for the proximal and medial-distal sections, respectively. We defined the end of the proximal zone on the basis of morphology, where a zone of overflows that occurs ~350 m from the vent; a point at which the first constriction is observed in the channel (Figure 1). This hybrid model now gives an excellent fit with measured width (Figure 2c), as well as effusion rate and velocity. Our main variable is now phenocryst content where we obtain best-fits with a starting phenocryst range of 25-30 %, which in turn effects our starting viscosity (3300-4500 Pa s), velocity (0.6-0.9 m/s) and effusion rate (4-6 m^3/s). Phenocryst contents that are lower and higher than this begin to produce model-generated widths, effusion rates and velocities that fit less poorly. However, this phenocryst range is approximately within one standard deviation of the mean from all published phenocryst contents for Etnean lavas [34±7 %, *Harris et al.*, 2005].

MODEL BEST-FIT

Using the output of the best fit model (Hybrid Model M3), we obtain model-derived down-flow profiles for cooling rate, crystallization rate, viscosity and velocity. For this best-fit, cooling rates vary from ~0.02-0.015 °C m^{-1} across the proximal section, to ~0.005 °C m^{-1} across the more effectively insulated medial-distal section (Figure 3a), to give a core temperature at the flow front (i.e. at a distance of ~1600 m from the vent) of ~1040 °C. Cooling results in crystallization rates that decrease from 4-6 x 10^{-5} volume fraction per meter across the proximal section, to 1-2 x 10^{-5} volume fraction per meter across the medial-distal section (Figure 3b), to give a total crystal (phenocrysts plus microphenocrysts) content at the flow front of ~35 %. These cooling and crystallization rates cause viscosity to increase from ~3800 Pa s at the vent to ~8000 Pa s at the distal section (Figure 3c), and compare with ~9400 Pa s measured for an Etnean flow by *Pinkerton and Sparks* [1978]. Likewise, yield strength increases down-channel from 160 Pa to 310 Pa, and again compares with 370 Pa obtained for Etna by *Pinkerton and Sparks* [1978]. Together, these rheological changes cause the flow to slow down, such that at the channel exit flow velocities decrease to ~0.15 m/s (Figure 3d).

CONCLUSIONS

We model a case whereby two thermal regimes effect the channel length. In the proximal section conditions are similar to those described in *Bailey et al.* [2006] and *Harris et al.* [2005] where hot crusts on a free flowing channel maximise heat losses.

These in turn maximise cooling rates. However, to allow flow to extend the full length of the channel we require a different thermal regime across the medial-distal section. This comprises a thick, stable, mature carapace of cool 'a'a clinker that effectively insulates the core and reduces core cooling and crystallization rates. The hybrid model provides an excellent fit with morphological data and implies cooling rates in the range 5-20 °C km^{-1} and viscosities in the range 10^3 –10^4 Pa s for flow in this channel active on steep (average = 20°) slopes. This testifies that flow dynamics cannot be assumed to be steady along the entire channel, but thermal and rheological regimes vary significantly down-channel, such that point measurements of surface thermal structure, core rheology and/or flow velocity will not be representative of the entire system. To better constrain and understand the complexity of this regime further flow-wide morphological [e.g. *Mazzarini et al.*, 2005; *Bailey et al.*, 2006] and thermal [e.g. *Calvari et al.*, 2005; *Lombardo and Buongiorno*, 2006] measurements are required.

REFRENCES

Bailey, J.E., A.J.L. Harris, J. Dehn, S. Calvari, and S.K. Rowland, (2006), The changing morphology of an open lava channel on Mt. Etna, *Bull. Volcanol.*, 68, 497-515.

Cashman, K.V., C, Thornber, and J.P. Kauahikaua, (1999), Cooling and crystallization of lava in open channels, and the transition of Pahoehoe to Aa, *Bull. Volcanol.*, 61, 306-323.

Calvari, S., M. Neri, and H. Pinkerton (2003), Effusion rate estimations during the 1999 summit eruption on Mount Etna, and growth of two distinct lava flow fields, *Journal of Volcanology and Geothermal Research*, *119*, 107-123, 2003.

Calvari, S., L. Spampinato, L. Lodato, A. J. L. Harris, M. R. Patrick, J. Dehn, M. R. Burton, and D. Andronico (2005), Chronology and complex volcanic processes during the 2002–2003 flank eruption at Stromboli volcano (Italy) reconstructed from direct observations and surveys with a handheld thermal camera, *J. Geophys. Res.*, 110, B02201, doi:10.1029/2004JB003129.

Chester, D.K., A.M. Duncan, J.E. Guest, and C.R.J. Kilburn (1985), *Mount Etna: The anatomy of a volcano*, Chapman and Hall (London).

Crisp, J.A., and S.M. Baloga (1990), A model for lava flows with two thermal components, *Journal of Geophysical Research, 95*, 1255-1270.

Crisp, J.A., and S.M. Baloga (1994), Influence of crystallization and entrainment of cooler material on the emplacement of basaltic aa lava flows, *J. Geophys. Res.*, 99(B6), 11819-11831.

Dragoni, M.A. (1989), A dynamical model of lava flows cooling by radiation, *Bull. Volcanol.*, 51, 88-95.

Dragoni, M.A., and A. Tallarico (1989), The effect of crystallization on the rheology and dynamics of lava flows, *J. Volcanol. Geotherm. Res.*, 59, 241-252.

Fink, J.H., and R.W. Griffiths (1992), A laboratory analog study of the surface morphology of lava flows extruded from point and line sources, *J. Volcanol. Geotherm. Res.*, 54, 19-32.

Giordano, D., and D.B. Dingwell (2003), Viscosity of hydrous Etna basalt: implications for Plinian-style basaltic eruptions, *Bull. Volcanol.*, 65, 8–14.

Gregg, T.K.P., and J.H. Fink (2000), A laboratory investigation into the effects of slope on lava flow morphology, *J. Volcanol. Geotherm. Res.*, 96, 145-159.

Harris, A.J.L., and S. Rowland (2001), FLOWGO: a kinematic thermo-rheological model for lava flowing in a channel, *Bull. Volcanol.*, 63, 20-44.

Harris, A., J. Bailey, S. Calvari, and J. Dehn (2005), Heat loss measured at a lava channel and its implications for down-channel cooling and rheology, *Geol. Soc. Am. Spec. Pap.*, 396, 125-146.

Hon, K., J. Kauahikaua, R. Denlinger, and K. Mackay (1994), Emplacement and inflation of pahoehoe sheet flows: Observations and measurements of active lava flows on Kilauea Volcano, Hawaii, *Geological Society of America Bulletin, 106,* 351-370.

Keszthelyi, L. (1995) Measurements of the cooling at the base of a pahoehoe flow, *Geophys. Res. Lett.*, 22, 2195-2198.

Keszthelyi, L., and S. Self, (1998), Some physical requirements of the emplacement of long basaltic lava flows, *J. Geophys. Res.*, 103(B11), 27,447-27,464.

Keszthelyi, L., A.J.L. Harris, and J. Dehn (2003), Observations of the effect of wind on the cooling of active lava flows, *Geophys. Res. Lett.*, 30(19), 1989, doi:10.1029/ 2003GL017994.

Kilburn, C.R.J. (1990), Surfaces of ‘a‘a flow-fields on Mount Etna, Sicily: morphology, rheology, crystallization and scaling phenomena, *in* Fink J.H., ed., *Lava flows and domes: emplacement mechanisms and hazard implications*, Springer (Berlin), 129–156.

Kilburn, C.R.J., and R.M.C. Lopes (1988) The growth of aa lava flow fields on Mount Etna, Sicily, *J. Geophys. Res.*, 93(B12), 14,759-14,772.

Kilburn C.R.J., and J.E. Guest (1993), ‘A‘a lavas of Mount Etna, Sicily, *in* Kilburn CRJ and Luongo G, eds., *Active Lavas: monitoring and modeling*, Univ. College of London Press (London), 73–106.

Jeffreys, H. (1925), The flow of water in an inclined channel of rectangular section, *Philosophical Magazine*, 49, 793–807.

Lombardo V., and F. Buongiorno (2006), Lava flow thermal analysis using three infrared bands of remote-sensing imagery: A study case from Mount Etna 2001 eruption, *Remote Sensing of Environment*, 101, 141-149.

Mazzarini, F., M.T. Pareschi, M. Favalli, I. Isola, S. Tarquini, and E. Boschi (2005), Morphology of basaltic lava channels during the Mt. Etna September 2004 eruption from airborne laser altimeter data, *Geophys. Res. Lett.*, 32, L04305, doi:10.1029/2004GL021815.

Mazzarini, F., M.T. Pareschi, M. Favalli, I. Isola, S. Tarquini, and E. Boschi (in press), Lava flow identification and aging by means of LiDAR intensity: the Mt. Etna case, Journal Geophysical Research, in press.

Moore, H.J. (1987), Preliminary estimates of the rheological properties of 1984 Mauna Loa lava, *U.S. Geological Survey Professional Paper*, 1350, 1569–1588.

Peck, D.L. (1978), Cooling and vesiculation of Alae lava lake, Hawaii, *U.S. Geological Survey Professional Paper*, 935-B, 1-59.

Pieri, D.C., and S.M. Baloga (1986), Eruption rate, area, and length relationships for some Hawaiian lava flows, *J. Volcanol. Geotherm. Res.*, 30, 29-45.

Pinkerton, H., and R.S.J. Sparks (1978), Field measurements of the rheology of lava, *Nature*, 276, 383-385.

Pinkerton, H., and R.J. Stevenson (1992), Methods of determining the rheological of magmas at sub-liquidus temperatures, *J. Volcanol. Geotherm. Res.*, 53, 47-66.

Pinkerton, H., and L. Wilson (1994), Factors controlling the lengths of channel-fed flows, *Bull. Volcanol.*, 56, 108-120.

Quareni, F., A. Tallarico, and M. Dragoni (2004), Modeling of the steady-state temperature in lava flow levees, J. Volcanol. Geotherm. Res., 132, 241-251.

Tanguy, J.C. (1973), The 1971 Etna eruption: petrology of the lavas, *Phil. Trans. R. Soc. Lond.*, 274, 45-53.

Wooster, M.J., R. Wight, S. Blake, and D.A. Rothery (1997), Cooling mechanisms and an approximate thermal budget for the 1991-1993 Mount Etna lava flow, *Geophys. Res. Lett.*, 24, 3277-3280.

Acknowledgements. AJLH was funded by NASA Grant NWG04GO64G.

Figure Legends

Figure 1 Digital Elevation Model derived from LiDAR data for Etna's east flnak [*Mazzarini et al.*, 2005]. The main flow channel-fed erupted during September 2004 is given in yellow, secondary overflow units in pale green. a: vent; b: zone of overflows; c: origin of secondary overflow units; d: flow toe.

Figure 2 Comparison of LIDAR-measured channel width (solid grey line) with model-derived channel widths (black dashed and solid lines). **a)** Model-derived widths for model 1 (poorly insulated flow – high temperature crust) where the widths produced by models 1.1 (M1.1: lightly crusted), 1.2 (M1.2: heavily crusted) and 1.3 (M1.3: $f_{crust} = 1$) are given by broken, thin solid and thick solid lines, respectively. **b)** Model-derived widths for model 2 (well-insulated flow) where the widths produced by model 2.1 (M2.1: $T_{crust} = 350$ °C, $f_{crust} = 1$), 2.2 (M2.2: $T_{crust} = 250$ °C, $f_{crust} = 1$) and 2.3 (M2.3: $T_{crust} = 150$ °C, $f_{crust} = 1$) are given by broken, thin solid and thick solid lines, respectively. **c)** Model-derived widths for model 3 (hybrid model: model 1.2 to 350 m, then model 2.3) where the widths obtained from model runs using phenocryst contents of 30 % (broken line), 27.5 % (thin solid line) and 25 % (thick solid line), are respectively given.

Figure 3 Model-derived down-flow profiles for a) core cooling rate, b) crystallization rate, c) viscosity and (d) velocity obtained using the best-fit hybrid model content (model 1.2 to 350 m, then model 2.3) with a 27.5 % phenocryst. The jump at ~350 m is

a result of moving from the poorly insulated model (model 1.2) to the well insulated model (model 2.3).

Table 1 Themal and rheological parameters used in applying the FLOWGO model to the 16th September 2004 Etna channel.

Parameter	Value	Source
Basal contact temperature	500 °C	*Keszthelyi* [1995]; *Wooster et al.* [1997]
Convective heat transfer coefficient	10-40 W m^{-2} K^{-1}	*Keszthelyi et al.* [2003]; *Harris et al.* [2005]
Crystallization rate	0.3 % K^{-1}	Calculated for Etna composition by [1]
Dense Rock Density	2600 kg m^{-3}	
Eruption temperature	1065 °C	*Bailey et al.* [2006]
Phenocryst content	34±7 %	Mean from all literature values for Etna [1]
Thermal conductivity	2.5 W m^{-1} K^{-1}	Calculated following *Peck* [1978]
Vesicularity	22 %	Mean from all literature values for Etna [1]
Viscosity of liquid upon eruption	930 Pa s	Calculated following *Giordano and Dingwell* [2003] using an eruption temperature of 1065 °C and ~0.37 wt % water [from *Tanguy*, 1973]

[1] Full data given in *Harris et al.* [2005]

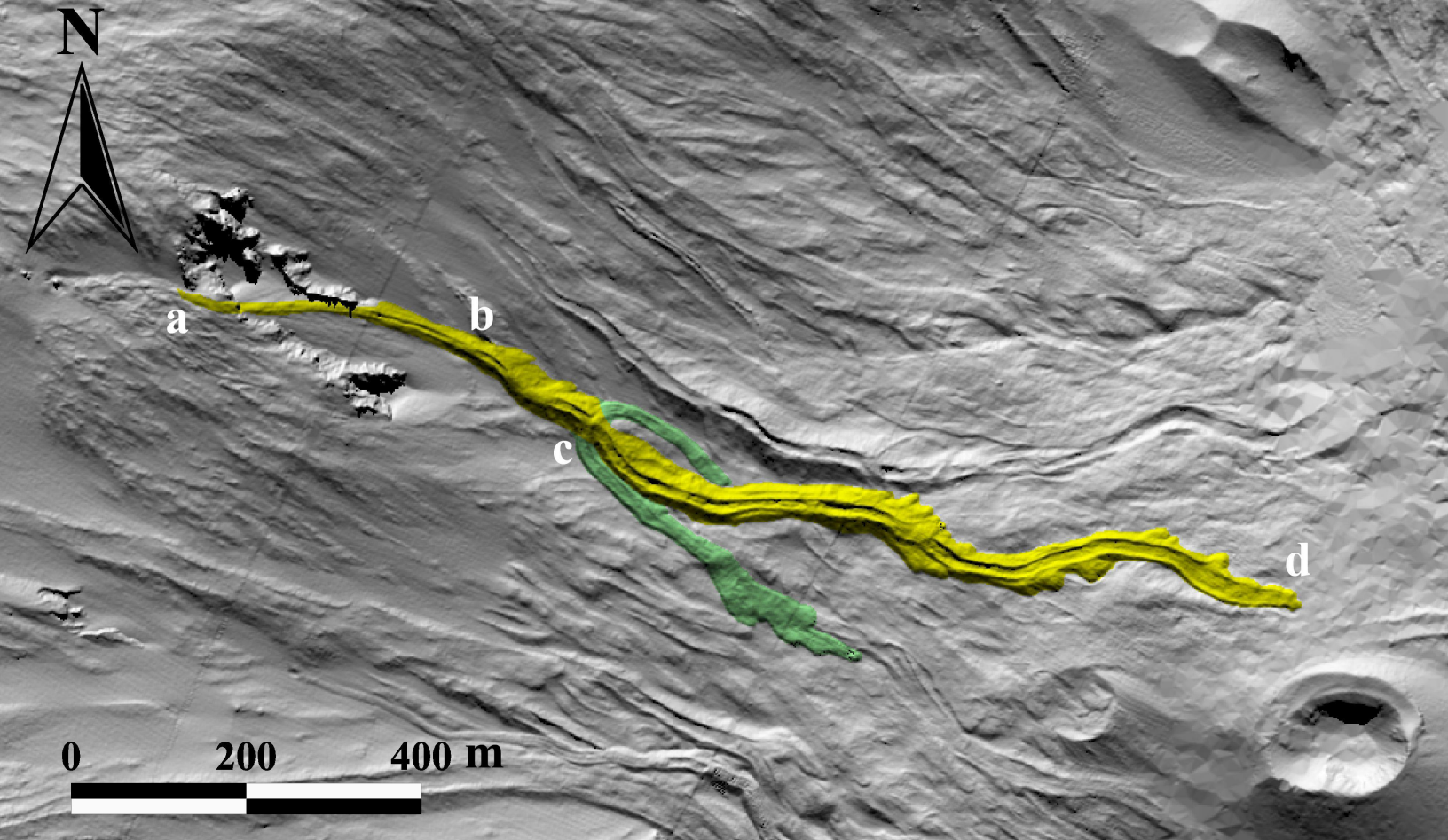
N
a
b
c
d
0
200
400 m

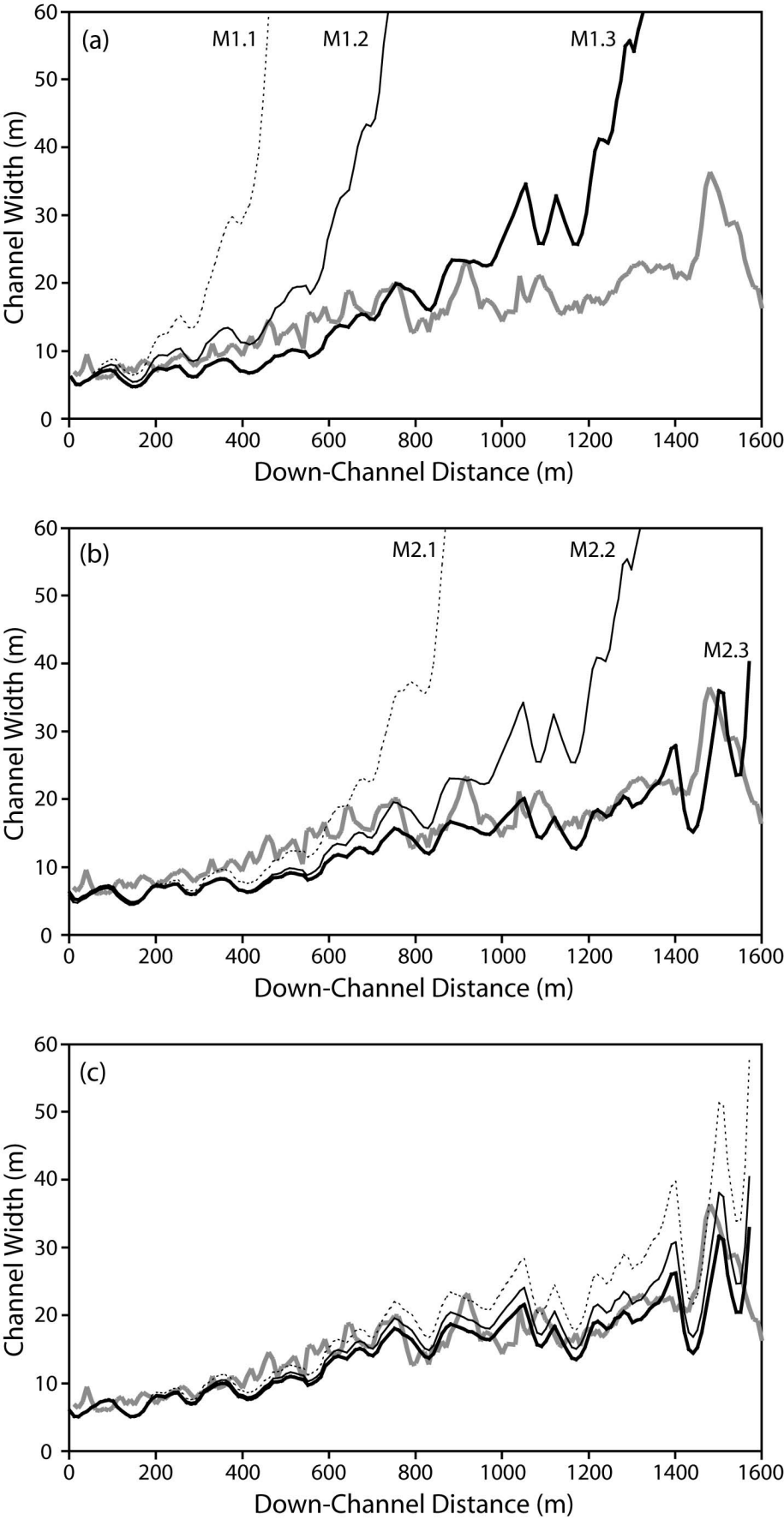
(a)
M1.1
M1.2
M1.3
Channel Width (m)
Down-Channel Distance (m)
(b)
M2.1
M2.2
M2.3
Channel Width (m)
Down-Channel Distance (m)
(c)
Channel Width (m)
Down-Channel Distance (m)

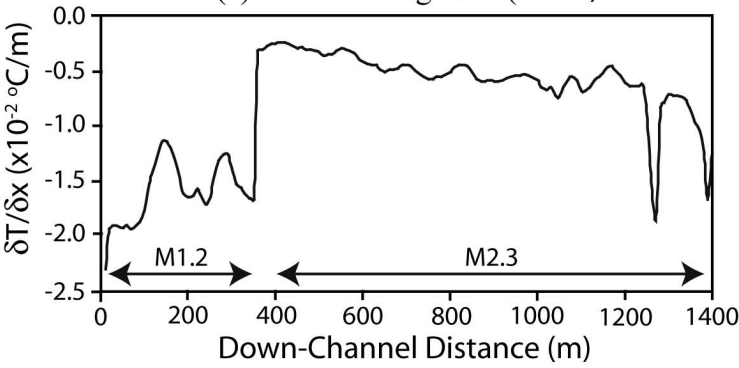
(a) Core Cooling Rate (δT/δx)
δT/δx (x10-2 °C/m)
0.0
-0.5
-1.0
-1.5
-2.0
-2.5
M1.2
M2.3
0
200
400
600
800
1000
1200
1400
Down-Channel Distance (m)

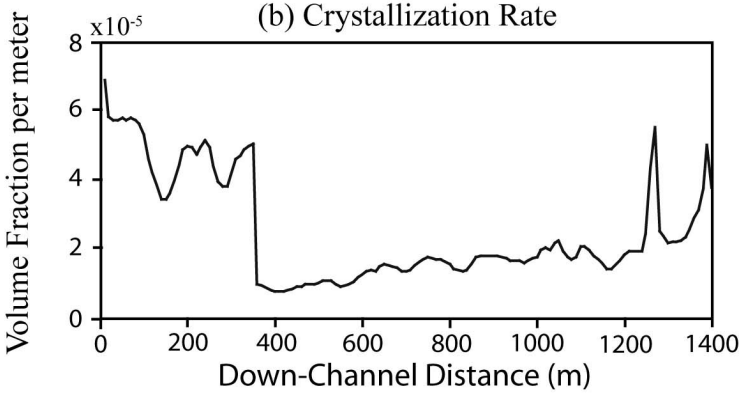
(b) Crystallization Rate
x10-5
Volume Fraction per meter
8
6
4
2
0
0
200
400
600
800
1000
1200
1400
Down-Channel Distance (m)

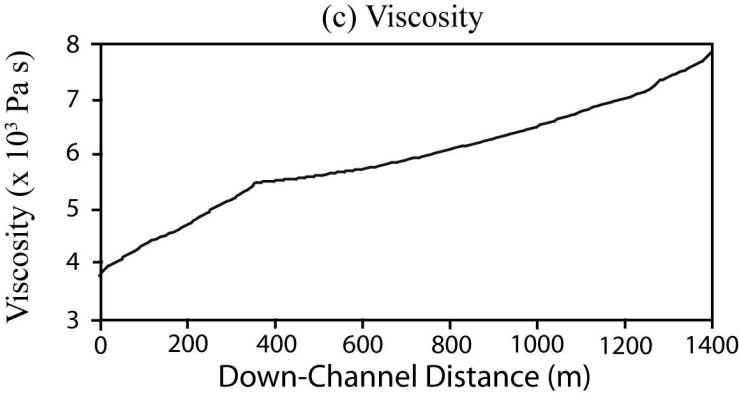
(c) Viscosity
Viscosity (x 10³ Pa s)
8
7
6
5
4
3
0
200
400
600
800
1000
1200
1400
Down-Channel Distance (m)

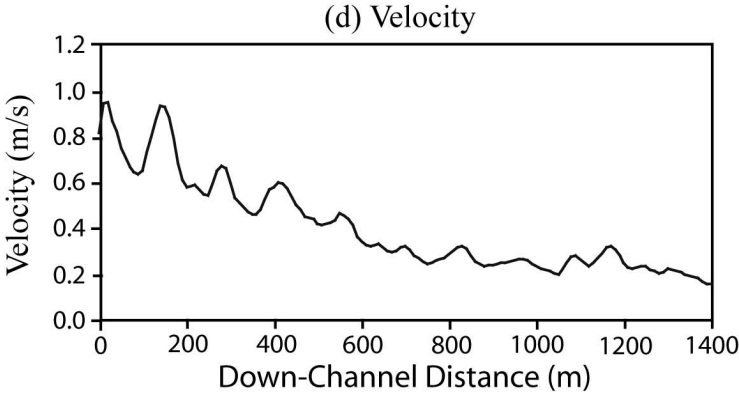
(d) Velocity
Velocity (m/s)
1.2
1.0
0.8
0.6
0.4
0.2
0.0
0
200
400
600
800
1000
1200
1400
Down-Channel Distance (m)